Engineering Solid Mechanics 8 (2020) 253-270

Contents lists available at GrowingScience

Engineering Solid Mechanics

homepage: www.GrowingScience.com/esm

Tribological, structural and mechanical characteristics of friction stir processed aluminium-based matrix composites reinforced with stainless steel micro-particles

Omolayo M. Ikumapayi[a*], Esther T. Akinlabi[a], Abhishek Sharma[b], Vyas Sharma[b] and Oluseyi P. Oladijo[c]

[a]*Department of Mechanical Engineering Science, University of Johannesburg, Auckland Park Kingsway Campus, Johannesburg, 2006, South Africa*
[b]*Department of Mechanical Engineering, Indian Institute of Technology, Kharagpur, India*
[c]*Department of Chemical, Materials & Metallurgical Engineering, Botswana International University of Science and Technology, Palapye, Botswana*

ARTICLEINFO

Article history:
Received 15 October 2019
Accepted 19 December 2019
Available online
19 December 2019

Keywords:
Aluminium-based matrix composite
Crystallite Size
Stainless steel powder
Tensile Strength
Wear

ABSTRACT

The efficacy of stainless-steel micro-particles on friction stir processed aluminium-based matrix composite (ABMC) was studied using tribological, mechanical and structural analysis tools. The stainless-steel powder (17-4PH) of average size 45 – 90 µm was used as the reinforcement particle. The parametric values employed during the fabrication of ABMC- AA7075-T651/17-4PH were the rotational speed of 1500 rpm and travel speed of 20 mm/min while the plunge depth and tilt angles used were respectively 0.3 mm and 3 degrees. Tribological study was carried out under the influence of dry sliding condition with varying loads of 20 N and 50 N using tribometer while the scanning electron microscope (SEM) was used to capture the wear track. Structural analysis was examined with the aid of x-ray diffraction (XRD). The tensile strengths of the fabricated ABMC were also tested and the fracture surfaces were studied using SEM analysis. The results from the study revealed that at higher loading of 50 N, the wear performance was significantly improved for the fabricated aluminium composite- AA7075-T651/17-4PH when compare with lower loading of 20 N. The tensile properties for the ABMC were also improved under the influence of the stainless steel microparticles. There was structural improvement in ABMC wherein the value for crystallite size was lowest while micro-strain, dislocation density, as well as full width at half maximum (FWHM), had the highest values over the FSPed AA7075-T651 and the parent material. The examined fractured surface of the fabricated composite was dominated with fine, network and equiaxed dimples with cup and cone attributes confirming superb interfacial bonding and that the failure mode was ductile.

1. Introduction

Aluminium-based matrix composites (ABMC) have been used in the manufacturing sectors for the fabrication of the following components such as brake drum, piston as well as cylindrical block whereby friction and wear play some cogent roles. Aluminium-based matrix composites (ABMCs) have been reported to have also found applications in most of marine, construction, automobile, nuclear, and aerospace sectors as one of the advanced and modern engineering and manufacturing materials used. ABMCs has several remarkable and excellent isotopic, structural, metallurgical, easy of fabrication, mechanical and electrochemical properties that made it suitable for the building of defence and military

* Corresponding author.
E-mail addresses: oikumapayi@uj.ac.za (O. M. Ikumapayi)

doi: 10.5267/j.esm.2019.12.001

equipment. These properties are not limited to low thermal expansion, high thermal conductivity, excellent wear-resistant, weldability, excellent formability, high fatigue strength, high creep resistant, promising damping capacities, high ductility as well as high stiffness (Huang et al., 2018; Ikumapayi et al., 2019a). It was reported that lower series of aluminium alloy has low thermal stability, poor corrosion-resistant, low hardness, as well as low tensile strength among others and such series, are pure aluminium (1xxx), copper-based (2xxx), manganese-based (3xxx), silicon-based (4xxx), magnesium-based (5xxx) so also series 6xxx (Ikumapayi & Akinlabi, 2019; Navaneethakrishnan & Ganesh, 2015; Vijaya Kumar, Madhusudhan Reddy, & Srinivasa Rao, 2015). These deficiencies have been overturned by high strength aluminium alloys which have improved structural, mechanical and chemical properties such series are zin-based (7xxx) as well as new series of 8xxx and 9xxx which are not so popular (Ikumapayi & Akinlabi, 2019; Rambabu et al., 2017). It has been established that lightweight materials such as magnesium, aluminium, and titanium offered dynamic and enterprising advantages over traditional steel metal as a result of their high specific strength and low density (Garcia et al., 2009; Vasco et al., 2018). It is, therefore, certain that in the future, steel might go into extinction wherein high strength and low-density materials such as aluminium, titanium, and magnesium might replace the steel. On this awareness and since titanium is very costly and magnesium is self-explosive, therefore aluminium might be the one that will likely replace steel in some of the prominent industries where steel functions today such as transportation, aerospace, automobiles, and defense sectors (Ikumapayi et al., 2019b; Sudhakar et al., 2016). The utilization of any of these engineering materials effectively and efficiently is very paramount for the manufacturing and designing of various structures, machines as well as vehicles, etc. It is essential to note that, engineering material must meet some fundamental integration of properties like toughness, strength, density, and stiffness. The combination of any of these properties may be absent from the conventional polymer, metal or ceramic. On this note, the fabrication of composites materials which will, therefore, have some amalgamated properties that conventional metal, ceramics or polymer were unable to meet. A structural material containing the combination of two or more constituents having a distinctive chemical or physical property which remains separate on macroscopic level within the final structure can be termed composite. A composite is a multiphase substance wherein the targeted properties can be produced by interfacial bonding between the reinforcement and the matrix substrate(Mistry & Gohil, 2017). It has been observed that aluminium and its alloy have been under-utilized industrial-wise due to some poor mechanical, structural and tribological properties embedded. On this awareness, report shows that surface modification of the base material is being altered via electron beam welding, thermal spraying as well as laser surfacing (Sudhakar et al., 2015). Nowadays, Friction stir processing has been adopted to cater for the complex methods of surface modification. Friction stir processing (FSP) was initially derived in 1999 from the work of (Gerlich, 2017; Mishra & Ma, 2005; Mishra et al., 2014) which took its root from a novel technique called friction stir welding (FSW) that was invented in 1991 and patented by the welding institute (TWI) of UK as a solid-state joining method. Afterwards, a large number of research papers have been published for investigating the mechanical properties, microstructure and quality of FSW and FSP components (Narasimharaju & Sankunny 2019; Kundu & Singh 2017; Jian et al. 2018; Aliha et al. 2016; Taheri-Behrooz et al. 2018; Torabi et al. 2018;2019 Akbari et al.2017; 2019, Shojaeefard et al. 2017; Behnagh et al. 2012; Shahraki et al. 2013; Asadi et al. 2012). Since the liberation of FSP in 1999, thousands of articles, hundreds of patents, thousands of textbooks as well as reviewed and peer-reviewed magazines had been in circulation which have been imparting life till date. It is worth knowing that lots of benefits emerge from FSP which include but are not limited to short-route of fabrication, densification, grain refinement, homogenization of precipitates of composites substance and aluminum alloys, Nugget zone homogeneity(Sanusi & Akinlabi, 2017), FSP has been well known for surface modification, significant and remarkable improvement in hardness, ductility, strength, increase fatigue life, as well as formability wherein the bulk properties are still intact (Fatchurrohman et al., 2018). Nonetheless, some difficulties are still being encountered in the course of modifying these surfaces using FSP, especially with reinforcement particles. It has been reported that backing plates usually stick to the workpiece when a thin or small diameter that is less than 1 mm is being processed, when proper optimum parameters are not being chosen, lots of flashes may be experienced during FSP techniques, lots of wear may be encountered during the fabrication of the

composites due to abrasive influence of the particles used for reinforcement (Ikumapayi et al., 2019c). Therefore, to achieve defect-free in the fabricated composites samples with good surface finish, experimental parameters must be adequately controlled. The processing parameters must be optimized to give a fabricated composite free of defects with high surface integrity. It is, therefore, imperative to note that the following parameters must be adequately controlled to give the best results such parameters include proper tool design, i.e. shoulder diameter geometry as well as pin profile while groove dimension in terms of depth and width should be well designed; also, machine variables must be controlled such as tool plunge depth, tool tilt angle, tool rotational speed, and tool traverse speed. In the same vein, amount of heat input and the method of heating and cooling must be controlled significantly while material properties must be known before and after the processing such as mechanical, chemical, thermal as well as electrical properties (Das et al. 2018; Ikumapayi et al., 2018a,b; Koli et al., 2014; Kumar et al. , 2017; Mishra & Ma, 2005; Sharma et al., 2015). Several researchers have done tremendous works on behaviors of aluminium alloy 7075 at different tapered conditions using various reinforcement particles ranging from metallic powders to agrowastes powders which are carried out experimentally and theoretically (Johannes & Mishra, 2007; Kubit et al., 2018; Padhy et al., 2017; Rana et al., 2016).

Patel et al. (2017) investigated the influence of polygonal pin geometry on the super-plasticity of aluminium alloy 7075 via friction stir processing. In this study, the following polygonal geometry was employed, hexagonal, square as well as pentagon pin profiles. The effects of pin profile on microhardness, grain refinement, as well as microstructures were examined. It was noted that the square pin profile produced fine grain with uniform microstructure without any defects in the stir zone while other pin profile has sticking of substrate on the pin profile ends resulting to non-uniform of microstructure. Selvakumar et al. (2017) fabricated aluminium matrix composite reinforced with stainless steel particulate. The percentages reinforcement was varied from 0, 6, 12 and 18 % by volume of stainless steel deposited in the groove with width (o.4, 0.8 and 1.2 mm) while maintaining a depth of 5.5 mm and length of 100 mm throughout the experiment. It was noted that 1600 rpm of rotational speed while 60 mm/min for a single pass. It was noted that produced aluminium composites showed equiaxed fine grains as a result of pining effects as well as dynamic recrystallization. It was further established that stainless steel particles employed yielded improved tensile strength while maintaining its ductility properties. The results have shown that UTS at 18 Vol% of stainless steel gave 293 MPa while at 0 vol% gave 222 MPa, this shows that stainless steel has influenced the mechanical properties. Similarly, the fracture surfaces of the AMC showed a network of dimples with superior interfacial bonding which can be attributed to the ductility properties of the fabricated composites. Feng et al. (2010) study the integrity of cyclic deformation in 6.35 mm thickness, 400 mm long and 80 mm wide, aluminium alloy 7075-T651 during friction stir welding. In this study, the microstructural analysis was carried out and significant grain refinement was achieved with dissolution of $(Mg(Zn,Al,Cu)_2)$ precipitates at the stir zone. It was observed that fatigue life and cyclic hardening were increased with increase in travel speed from 100 mm/min to 400 mm/min while little effects were noticed when rotational speed was increased from 800 rpm to 1200 rpm. It was noted that stress amplitude increased while plastic strain amplitude decreased during friction stir welding between 800 rpm and 1200 rpm rotational speed.

Sert and Celik (2014) studied the wear properties of the aluminium alloy Al7075-T651 under the influence of Silicon Carbide (SiC) particles via friction stir processing. In this study, varying load of 2, 4 and 5 N were tested using ball-on-disk configuration with sliding speed of 2.5 cm/s while friction stir processing parameters that were employed are 710 rpm of constant rotational speed wherein the traverse speed used are varying with 20 mm/min, 40 mm/min and 56 mm/min. It was noted that at 2 N applied force and 40 mm/min, reinforced aluminium matrix composite produced the best wear properties when compared with unreinforced samples. Jain et al. (2018) studied wear behaviour alongside with the mechanical properties' aluminium-based (5053) matrix composites reinforced with tri-particles containing B_4C/SiC/TiC using friction stir processing. The results show that reinforcing with B_4C produced the least grain size of 3.80 μm followed by SiC given 4.90 μm size while TiC produced 5.50 μm and the base metal has the highest grain size of 40.90 μm. The wear rate for AA5083- B_4C was found

to be the least which was 18.00 x 10^{-5}mm^3/Nm with hardness of 132.56Hv whereas AA5083-TiC produced 24. 25 x 10^{-5}mm^3/Nm wear rate making the second-best particles that can resist wear with hardness of 118.25Hv and that of AA5058-TiC performed least among the tested samples with 22.28 × 10^{-5}mm^3/Nm wear rate and 114.55Hv hardness. Kishan et al. (2018) investigated the tribological behaviour of aluminium alloy 6061-T6 using nanoparticles of TiB_2 during friction stir processing. In the study, the authors reinforced Al6061-T6 with different percentages by volume of 35 nm TiB_2 which are 2 vol %, 4 vol %, 8 vol % of TiB_2. It was noticed that at 4 % by volume of TiB_2, wear resistance was said to be high with microhardness of 132HV as against the base metal of 104HV. More debris was noticed at 8 vol% as against other reinforcement.

This present work focused on the study of tribological behaviours such as wear properties, mechanical behaviours such as tensile and fracture mechanism as well as structural behaviours such as crystal structure and grain size measurements under the influence of 17-4Ph stainless steel powder on the fabricated aluminium 7075-T651 alloy.

2. Materials and Methods

2.1 Materials

Commercially available 6mm thickness rolled aluminium alloy 7075-T651 metal plates were used in this study with dimensions 300 × 125 × 6 mm^3. The spark spectrometric analysis of as-received base metal was carried out and the result is documented in Table 1 and the mechanical properties in as received form are Shear Modulus (26 GPa), Brinell Hardness (150), Fatigue strength (160MPa), shear strength (330 MPa), Elastic Modulus (70 GPa), Poisson's Ratio (0.32), Yield Strength (500 MPa) and Ultimate tensile strength (UTS) (570 MPa). The base material was reinforced metallic micro-particles containing 17-4 PH stainless steel powder. The powder was received in average size 45 – 90 µm. The morphology of the powder was studied using scanning electron microscope (SEM) and its elemental compositions were also captured by the Energy Dispersive X-ray Spectrometer (EDXS). The powder characterizations were carried out at a SEM magnification of 200x, with a beam intensity of 10 and accelerating voltage of 20kV in which the working distance was 16.25 mm. The SEM Image and it corresponding EDXS are presented in Fig. 1.

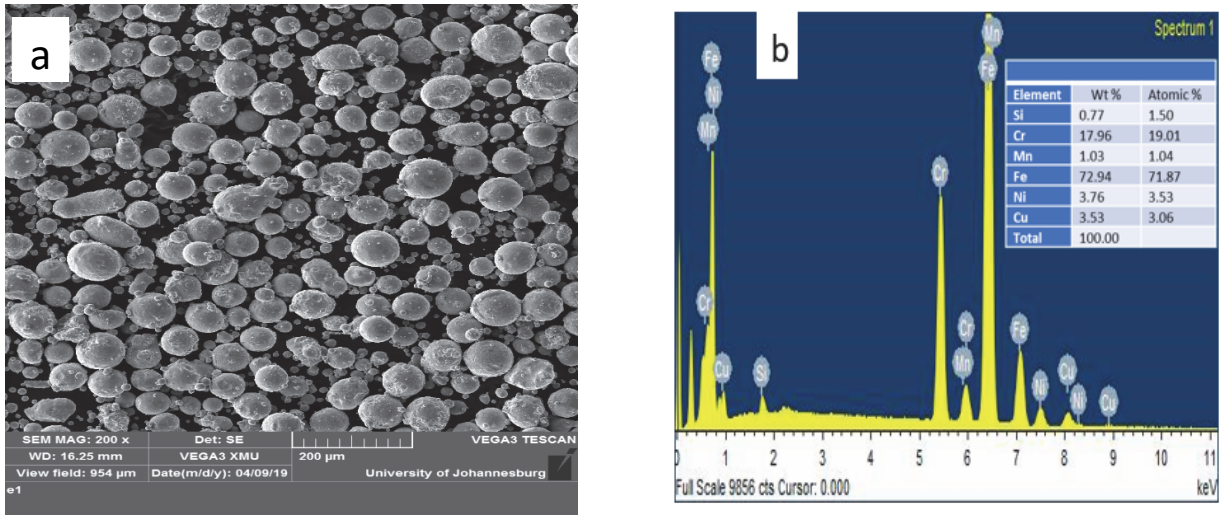

Fig. 1(a). SEM Images of 17-4 PH Stainless steel powder (b) its EDS

The friction stir processing was conducted on a two-tons numerically controlled friction stir welding machine (see Fig. 2a) manufactured by ETA Banglore, India Ltd. A microchannel (groove) was created on the plates with dimensions, 3.5 mm depth, 280 mm length and 2. 0 mm width, while AISI H13 hot-working tool steel was employed for stirring and mixing. The processing tool has 18 mm shoulder

diameter, 5 mm pin diameter, and 5 mm pin length. Two passes were carried out on the optimum processing parameters with 100 % inter-pass overlap. The first pass was done on the processing parameters having 100 mm/min travel speed and 1000 rpm rotational speed with pinless processing tool of 18 mm shoulder diameter. The second pass was done with 20 mm/min travel speed and 1500 rpm rotational speed with plunge depth of 0.1 for first pas and 0.2 for second pass and tilt angle of 3°. The schematic three – dimensional model of the friction stir processing is depicted in Fig. 2b.

Table 1. Chemical composition AA7075-T651 aluminum alloy

Elements	Mg	Fe	Ti	Si	Mn	Zn	Cu	Cr	Al
Wt.% Composition	2.8	0.15	0.02	0.05	0.01	5.92	1.93	0.193	**Balance**

Fig. 2a. NC-controlled FSW machine

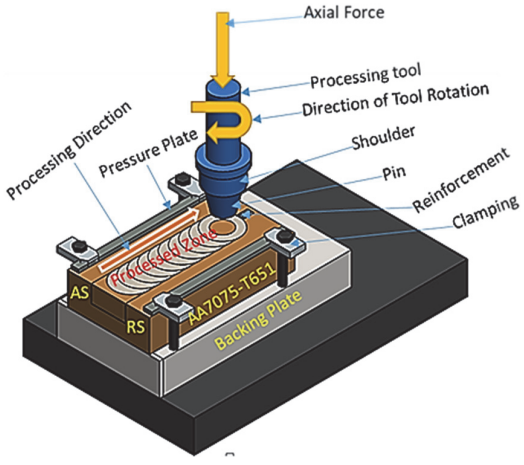

Fig. 2b. Schematic 3D model of FSP

2.2 Tribological Study – Wear Behaviours

A Cyclic and ball on flat disc wear test was conducted on the aluminium alloy with dimension 24 mm × 10 mm × 6 mm size. The test was carried out as dry and unlubricated using Rtec Universal tribometer MTF 5000 which has the capability of imaging through three-dimensional in-line profilometers. The system software was made of MF17 for data acquisition. The experiment was conducted in-line with the ASTM G133-05 standards (Erinosho et al., 2017) and this test was carried out on three test samples in triplicate to ensure reproducibility and this is to measure the consistency of the results. The tested samples are base metal - AA7075-T651, FSPed AA7075-T651, and FSPed AA7075-T651/17-4Ph AMC. Two different forces were used in this experiment and they are 20 N Load and 50 N Load. The following parameters were measured as acquired, coefficient of friction (COF), wear track, wear volume, friction force for all the tested samples while wear resistance and wear rate was computed. The test samples were carried under the influence of ambient temperature of 25 °C. The parameters engaged during the tribological experimental procedures were reported in Table 2.

Table 2. Tribological Experimental Parameters

Item	**Parameter**
Lubrication	Dry/unlubricated
Loads	20 N, 50 N
Ball-type	Alloy steel E52100
Sliding Distance	3 mm, 5 mm
Loading type	Constant
Sliding Speed	3 mm/s
Wear Type	Cyclic, ball-on-Flat test
Ball Grade	25
Sliding time	5 mins
Ball Size	6.35 mm

2.3 Structural Study – XRD Analysis

The X-ray diffraction (XRD) analysis was performed using the PHILIPS X'Pert (model number 12NC: 943003040601) operated at PW: 3040/60, 240V, 8.5KVA, and 50Hz and with the specifications in **Table 3**. XRD test was carried out on the base metal as well as fabricated samples to confirm the crystal structure and mineralogical compositions of the samples used. The XRD was acquired using an automatic divergence slit; i.e., an irradiated sample length that is independent of the Bragg angles ((2θ) in degree). The diffraction patterns and crystal phases at different samples were obtained and presented. In the same vein, the following parameters were computed grain size, dislocation density, as well as micro-strain by using the Scherrer method.

Table 3. Diffractometer machine specification

Property	Specification
Current	30mA
Excitation voltage	40kV
Scanning rate	1.0000 deg/min (2Θ/seg)
scan range (2θ)	Between 5° and 90°
K	0.94
Kα radiation	λ = 1.5406 Å
k∝ radiation	λ = 1.39225 Å
step width	0.0100 deg

2.4 Mechanical Characteristics – Tensile Test

The tensile test was carried out following ASTM B557M-10 standard (Ikumapayi et al., 2015). The test samples were carried out on the Xforce P-type Zwick/Roell Z250 Tensile testing machine. Substandard test samples of 100 mm long with thickness of 6 mm were used. The tested samples were carried out in triplicate each to ascertain the level of accuracy and reproducibility and mean values were taken and recorded. The test was conducted at a temperature of 25 degrees. The fracture surfaces of the tested samples were examined using SEM. The processed zone showing the section of the tensile sample is as shown in Fig. 3a while the sectioned tensile sample is illustrated in Fig. 3b and the photograph of machined tensile samples is presented in Fig. 3c with its fractured surface in Fig. 3d.

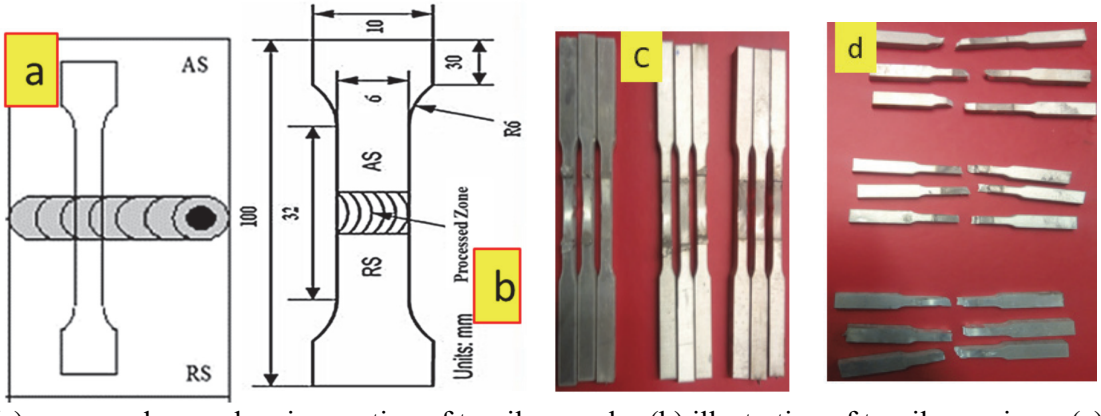

Fig. 3. (a) processed zone showing section of tensile samples (b) illustration of tensile specimen (c) photograph of tensile samples (d) photograph of the fractured surface of tensile samples

3. Results and discussion

3.1 Wear Behaviour Examination

Wear has been termed as gradual removal or deformation of material from the surface of a solid substrate and this can either caused by corrosion types (chemical wear) or erosion type (mechanical wear)

(Ikumapayi et al., 2018). There are several forms of wear categories; they are Surface Fatigue wear, Erosion wear, Adhesive wear, Corrosion and oxidation wear, abrasive wear, cavitation and fretting wear (Bhaskar et al., 2018). In order to reduce cost and loss of material at the same time prolonging the service life of produced aluminium matrix composites has endeared the study into the mechanism of wear properties. In this current research work, non-lubricant, dry sliding wear were experimented on AA7075-T651 (Base Metal), FSPed AA7075-T651(Processed base metal) as well as on AA7075-T651/17-4PH AMC in order to evaluate the efficiency of the reinforced 17-4PH particle in alleviating wear losses. It is imperative to mention that the following data were measured as acquired wear width, volume loss, wear depth, and coefficient of friction (COF) while wear rate, wear resistance, and frictional force was computed using Eqs. (1-2) (Deuis et al., 1997; Sudhakar et al., 2015)

$$V_w = \frac{C_w dL}{3h} \tag{1}$$

where C_w = Wear Coefficient; V_w = Wear Volume; L = Load applied;
h = Substrate bulk hardness, d = Sliding distance

$$Volume\ loss\ (mm^3) = \left(\frac{Weight\ loss\ (g)}{Density\ (\frac{g}{mm^3})}\right) \times 1000 \tag{2}$$

The SEM micrographs reported were showing the measured values of wear trace. The diagram illustrating wear track is depicted in Fig. 4a, the wear depth, wear cross-sectional area, as well as wear width was represented. Similarly, the schematic of tribometer experimental setup is displayed in Fig. 4b. The wear widths were recorded three times to ensure consistency of the results as shown in the SEM micrographs as displayed in Fig. 5 and this is to ascertain reproducibility and the mean value was recorded for each wear width of the tested sample. The morphologies at 100 x SEM image magnification of the worn surfaces for AA7075-T651 (Base Metal), FSPed AA7075-T651(Processed base metal) as well as on AA7075-T651/17-4PH AMC at different loading conditions of 20 N and 50 N were reported in Fig. 5.

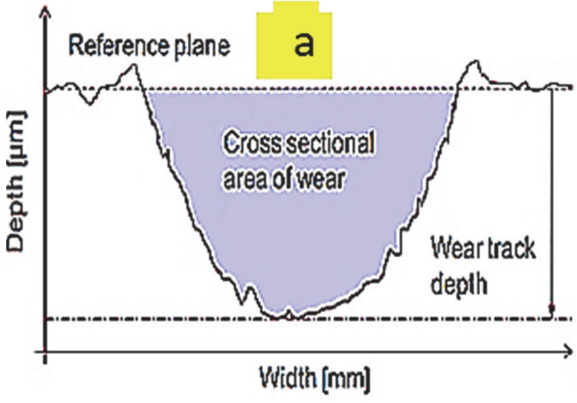

Fig. 4a. Illustration of wear track

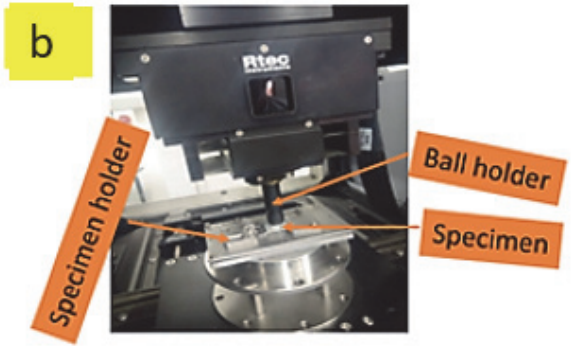

Fig. 4b. Tribometer Experimental setup

It is interesting to mention that wear rate was computed using equation vi and wear resistance was calculated using equation vii (Baruwa et al., 2018; Kumar & Wani, 2017; Sudhakar et al., 2015) while the coefficient of friction (COF) was derived from following relations for each tested and fabricated sample (Jeyaprakash et al., 2019).

$$\text{Wear rate } (mm^3/m) = \left(\frac{Volume\ loss\ (mm^3)}{Sliding\ distance\ (m)}\right) \times 1000 \tag{3}$$

$$\text{Wear resistance } (m/mm^3) = \left(\frac{Sliding\ distance\ (m)}{Volume\ loss\ (mm^3)}\right) \times 1000 \tag{4}$$

$$\text{Coefficient of friction } (\mu) = \frac{Friction\ Force\ (F_f)}{Applied\ Load\ (L)} \quad (5)$$

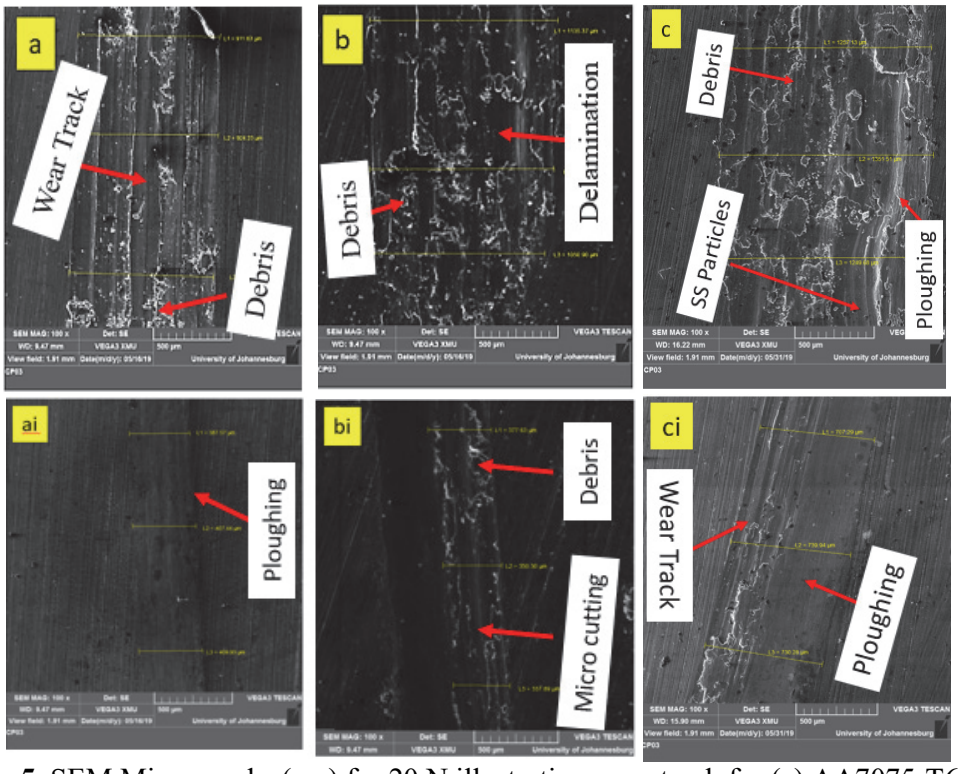

Fig. 5. SEM Micrographs (a-c) for 20 N illustrating wear track for (a) AA7075-T651 (b) FSPed AA7075-T651 (c) AA7075-T651/17-4PH; (ai-ci) for 50 N: (ai) AA7075-T651 (bi) FSPed AA7075-T651 (ci) AA7075-T651/17-4PH

3.2 Influence of Applied Loads on Wear Characteristics

Tables 4 and 5 show the values of data measured, computed and recorded for wear test at an applied load of 20 N and 50 N respectively. The parametric values used when 20 N applied load was applied were sliding distance, cyclic time and speed of 3 mm, 5 minutes and 3 mm/s respectively conducted at room temperature. Also, when 50 N applied load was applied, the following parametric factors were applied, sliding distance, speed and time which are 5 mm, 3 mm/s and 5 mins respectively. The SEM images of the tested samples representing the worn surfaces are depicted in Fig. 5. It was noticed that when 20 N force was applied, more debris was observed than when 50 N force was applied and this may due to the excessive heat generated during the sliding, and cyclic movement of the steel ball on the substrate being tested and this also leads to degeneration of plastic deformation on mechanical properties and softening the wear paths (Dinaharan et al., 20171), by so doing cleaning off the debris generated along the wear track and was in consensus with the work reported in (Boromei et al., 2006). It was observed that the mean values for wear width when 50 N applied force were larger than that of 20 N applied force as evidence on the SEM images in Fig. 5. Delamination was more conspicuous in the wear track when an applied force of 20 N was used. Figs. 6 and 7 respectively represent the 20 N applied force and 50 N applied force of wear tracks with their respective profiler at different tested samples.

Table 4. Wear experimental data obtained at an applied load of 20 N

Parameters	20 N, 5 mins, 3 mm and 3 mm/s						
Sample	Wear Depth (mm)	Friction Force (N)	Wear Volume (mm^3)	Wear width (μm)	Wear Resistance (m/mm^3)	COF	Wear Rate (mm^3/m)
AA7075-T651	0.0213	9.360	0.049940	920.22	60072.09	0.4680	16.647
FSPed AA7075-T651	0.0201	9.136	0.042313	1099.76	70900.19	0.4568	14.104
AA7075-T651/17-4PH	0.0176	8.418	0.032578	1286.11	92086.68	0.4209	10.859

Table 5. Wear experimental data obtained at an applied load of 50 N

Parameters	50 N, 5 mins, 5 mm and 3 mm/s						
Sample	Wear Rate (mm^3/m)	Wear Depth (mm)	Wear Volume (mm^3)	Wear width (μm)	Wear Resistance (m/mm^3)	Friction Force (N)	COF
AA7075-T651	5.672	0.0288	0.028358	401.65	176317.09	9.845	0.1969
FSPed AA7075	2.878	0.1135	0.014390	355.27	347463.51	6.600	0.1320
AA7075-T651/17-4PH	2.275	0.0218	0.011374	725.83	439599.09	5.840	0.1168

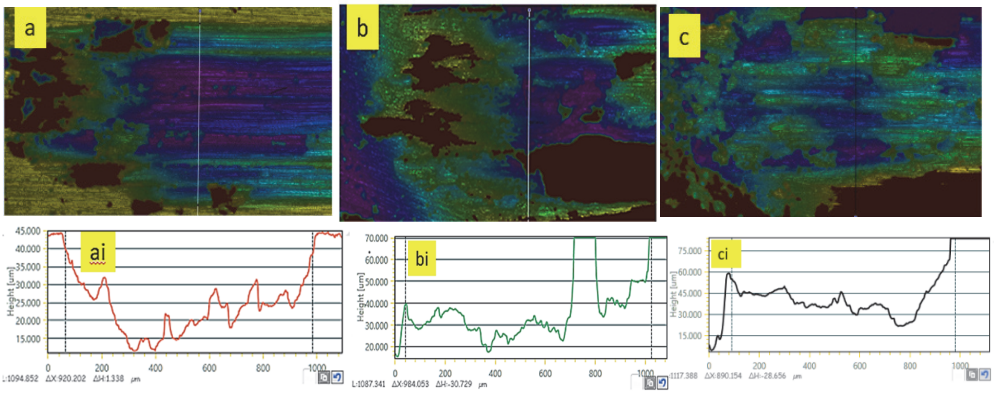

Fig. 6. 2D and Profiler for Wear track at 20 N (a) AA7075-T651 (b) FSPed AA7075-T651 (c) AA7075-T651/17-4PH

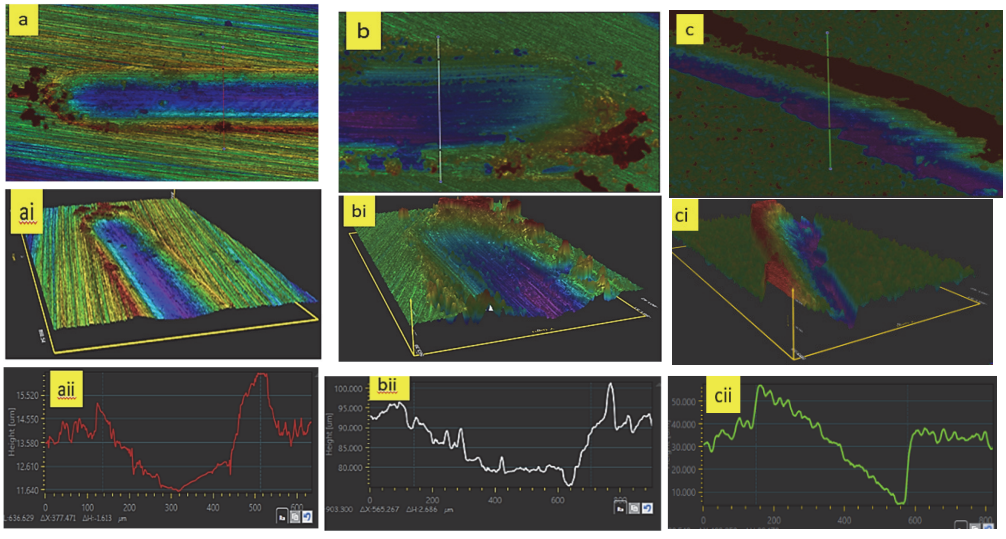

Fig. 7. 2D, 3D and Profiler for wear track at of 50 N (a-aii) AA7075-T651 (b-bii) FSPed AA7075-T651 (c-cii) AA7075-T651/17-4PH

In order to establish the potency of the reinforcements used in this study on wear behaviours, a comparative analysis was carried out on both reinforcements particles with reference to applied load and wear parametric properties. At applied load 20 N in Table 4, the wear volume for unprocessed base metal – AA70075-T651was measured to be 0.049940 mm^3 which was higher than when 50 N load is applied on the same substrate, in this case was 0.028358 mm^3 as depicted in Table 5. By this the volume loss in materials was minimized at higher load. On the same substrate – AA7075-T651, it was noticed that wear rate was higher at 20 N applied load than when 50 N load is applied which amounted to 16.647 mm^3/m and 5.672 mm^3/m respectively and wear resistance was larger when 50 N applied load was used which gave 176317.09 m/mm^3 and 60072.09 m/mm^3 when 20 N was applied. When relating with wear depth, the larger force of 50 N gave higher depth on unprocessed base metal – AA7075-T651 which was 0.0288 mm as against 0.0213 mm when 20 N force is applied. The coefficient of friction (COF) was more at 20 N force applied than at 50 N force applied which were 0.4680 and 0.1969. Fig. 8 shows the plot of tribological parametric values with reference to applied load on the tested samples. On examining the friction stir processed of base metal – FSPed AA7075-T651, one could see that at 20 N force applied, the volume loss was recorded to be 0.042313 mm^3 while that of 50 N applied load was 0.014390 mm^3, which means that at higher load, minimum volume loss was noticed. At this point, the wear resistance was largely noticed at 50 N applied load which was 347463.51 m/mm^3 while at 20 N applied force, it was 70900.19 m/mm^3. The wear rate was far higher in FSPed AA7075-T651 when 20 N force was applied which gave 14.104 mm^3/m and was so minimal at 50 N force applied with a value of 2.878 mm^3/m. The COF at 20 N and 50 N was 0.4568 and 0.1320 respectively. This also tells that higher loading performed better than lower loading in all instances for FSPed AA7075-T651 as also evidenced in the work reported by Asuke et al. (2014).

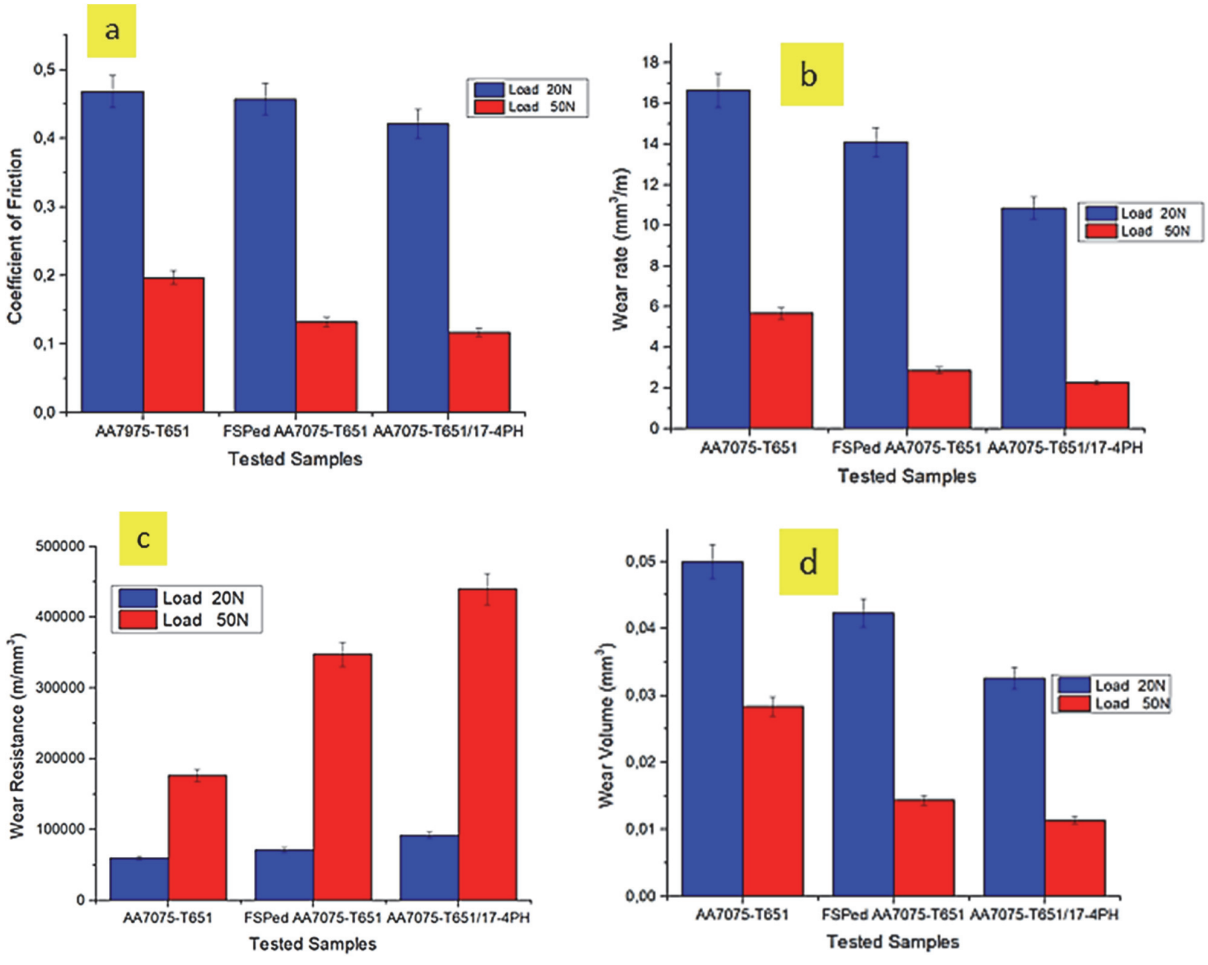

Fig. 8. Plots of tribological parameters

3.3 Structural Study – XRD Analysis Results

Table 6 shows the results generated from XRD analysis, the crystallite size was extracted from the data acquired and confirmed using Scherrer and Wilson Equation as represented in Eq. (6), the line broadening which is FWHM- full width at half maximum was also acquired and recorded, the d spacing was extracted from the data acquired from the highest peak of the spectrum and was confirmed using Bragg's formula presented in Eq. (7). The micro-strain (ε) was calculated using equation formulated by Williamson hall as depicted in equation (8) and lastly, the dislocation density (δ) was using the formula presented in Eq. (9) (Offor et al., 2015; Pandey et al., 2017).

$$C = \frac{k\lambda}{\beta Cos\theta} \tag{6}$$

$$\mathrm{d} = \frac{n\lambda}{2Sin\theta} \tag{7}$$

$$\varepsilon = \frac{\beta cos\theta}{4} \tag{8}$$

$$\delta = \frac{1}{C^2} \tag{9}$$

where θ = Bragg's angle; λ = wavelength, n=1 and β = FWHM.

Table 6: XRD data analysis Results

Samples	FWHM,∝ (°)	Crustal Plane	2θ (°)	Micro Strain (ε) × 10^{-2}	d spacing (Å)	Dislocation density (δ) (Lines/m^2) × 10^{14}	Crystallite size, C (nm)
AA7075-T651/17-4PH	0.240	111	39.9	5.6399	2.260	7.1491	37.4
FSPed AA7075-T651	0.213	111	38.1	5.0381	2.364	5.8912	41.2
AA7075-T651	0.180	111	38.1	4.2535	2.364	4.2164	48.7

X-ray diffraction analysis was used in this study to detect phases, crystal structure, diffraction pattern as well as evolving crystalline phases (Pandey et al., 2017). Fig. 9 shows the various structural pattern with different crystal phases embedded. There are three different samples tested as depicted in Fig. 9, unfabricated parent material – AA7075-T651 having a peak colour of red, fabricated parent material – FSPed AA7075-T651 with a peak colour of blue and also fabricated aluminium-based matrix composite – AA7075-T651/17-4PH with a peak colour of orange located at the position of in 2θ values. There are common peaks to all the tested samples as noticed in Fig. 9 which are (111), (200), (220), (311) and (222) wherein the fabricated composites had some additional peaks which are (100), (110), (210), and (300) which was the effect of the reinforcing microparticles. The fabricated AA7075-T651/17-4PH possessed the lowest value of crystallite size with 37.4 nm where the dislocation density, d spacing, microstrain as well as FWHM were seen with the highest values in the fabricated AA7075-T651/17-4PH which implies that stainless steel microparticles greatly improved the structural properties of the fabricated composite over the control experiments – FSPed AA7075-T651 and the parent material – AA7075-T651 this was also in line with the work of Hao et al. (2019) and Kurgan (2014)

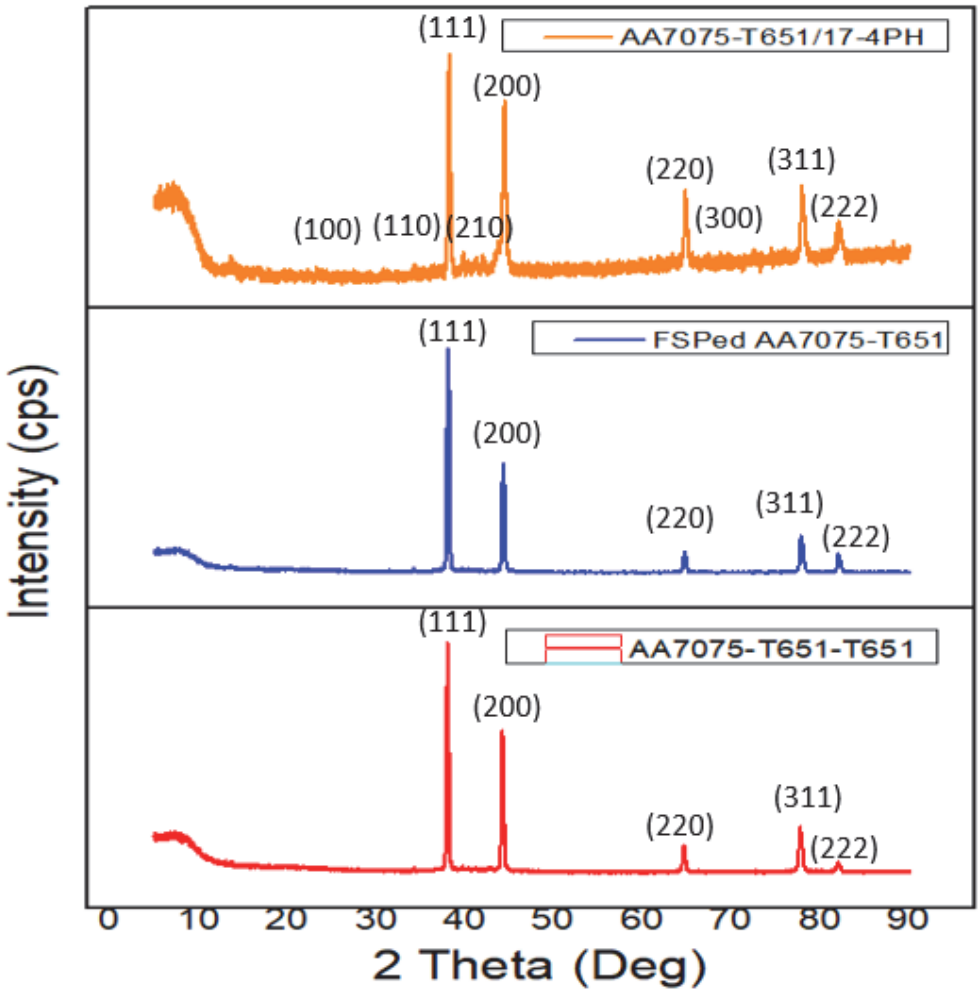

Fig. 9: XRD Pattern for the fabricated Samples

3.4 Tensile results and Fracture Surface Mechanism

Table 7 shows the tensile results of the tested samples. The following parameters were measured and recorded, tensile strength, fracture force, elongation as well as ultimate tensile strength. There was an improved in mechanical properties when stainless steel was used as reinforcement in aluminium alloy 7075. Table 6 shows that AA7075-T651/17-4PH AMC has the highest tensile strength of 613.58 MPa with ultimate tensile strength (UTS) of 622.22 MPa while the parent material has a very close value with that of fabricated AMC having 620.90 MPa UTS with 570.73 MPa tensile strength. The processed parent material exhibited the least value of mechanical properties with its values having close proximity to that of the parent material. The elongation is more in AA7075-T651/17-4PH AMC with 14.30 % indicating that is more ductile than the other tested samples followed by parent material with 9.73 % while FSPed AA7075-T651 having 7.22 %. The fracture force was also more in AA7075-T651/17-4PH with a value of 25 kN this may be as a result of its UTS and tensile value. The least values in friction stir processed AA7075-T651 (without reinforcement) may be as a result of inhomogeneous stirring and mixing which is evident in the result of its fractography. The fracture parts of the tensile specimens were taken for examination under the scanning electron microscopy (SEM). The fractographic were taken, studied and reasonable conclusions were drawn out. The tested samples were the parent material (PM) – AA7075-T651 which is unprocessed sample under tensile loading (control experiment 1), the second specimen tested was processed parent material (PPM) without reinforcement – FSPed AA7075-T651 (control experiment 2) while the last specimen subjected to tensile loading was the aluminium-based matrix

composite (ABMC) under the influence of 17-4PH stainless steel micro-particles – AA7075-T651/17-4PH. There some factors that affect the fabrication of ABMC such as the nature of the reinforcement particles, the sizes of the reinforcement particles such as nano, micro, and macro scales, substrate used in the fabrication, volume of the reinforcement applied, as well as matrix interfacial bonding (Hao et al., 2019).

Table 7. Mechanical properties of the Tested Samples

Tested Samples	Tensile Strength (MPa)	Fracture Force kN	Ultimate Tensile Strength (MPa)	Elongation (%)
AA7075-T651	570.73	22.35	620.90	9.73
FSPed AA7075-T651	559.07	20.04	603.83	7.22
AA7075-T651/17-4PH	613.58	25.40	622.22	14.30

Fig. 10a-c was characterized with dimple structure which indicates that they are ductile fractures. An elongated and large dimple was noticeable in Fig. 10a with appreciable lip region at the outer boundary of the final fracture, these noticeable fibrous features are indication that the crack propagation occurred slowly (Sharma et al., 2018) while there was bimodal distribution in Fig. 10b which is more of transition from brittle to ductile nature of the material, this type of failure can be caused by impact loading of the matrix which resulted in low ductility, hence formed "Rock Candy fracture" as noticed in Fig. 10b while Fig. 10c which was reinforced with micro-particle of stainless steel has large volume of dimples-induced grain. The cracking pattern exhibited what is termed equiaxed dimples with prominent cup and cone features, typical behaviour of ductile materials and this was in conformity with the study in (Dinaharan et al., 2017b). This plastic deformation was as a result of ample load resulting to ductility behaviour of the matrix composite and this can be termed relaxation cracking with fine dimples covered the grain boundaries and this was also in conformity with study in (Ikumapayi et al., 2018). It has been established that any structural and constructional part that is capable of withstanding a load only to certain value, can either break or deform. If the deformation is visible to naked eye, that is, extensive shear lips or necking – this can be referred to as ductile fracture or yielding as depicted in Fig. 10. The constructional and structural material such as aluminium alloy 7075-T651 must be strong enough and be ductile in order to withstand any sudden, impact or shocking overload.

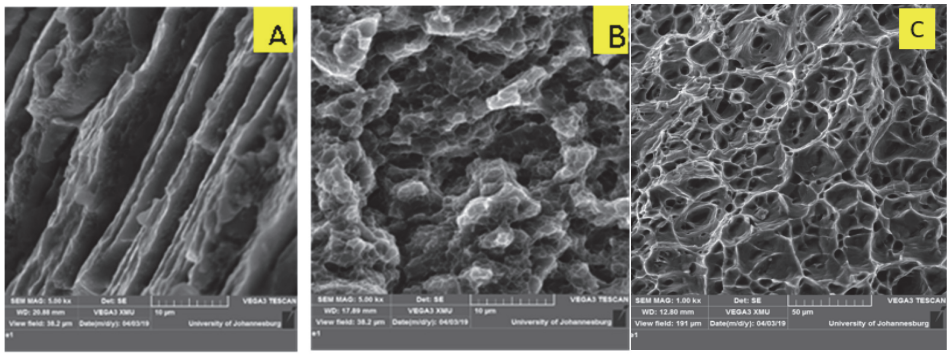

Fig. 10: Fractography of the tensile tests fractured surfaces (a) AA7075-T651 (b) FSPed AA7075-T651 (c) AA7075-T651/17-4PH AMC

4. Conclusion

In this report, experimental analysis of fabricated aluminium-based matrix composite (ABMC) – AA7075-T651/17-4PH was studied structurally, mechanically and tribologically with reference to the parent material (PM) and processed parent material (PPM). It was established from the tribological point of view involving two different loading conditions of 20 N and 50 N applied force. The wear properties

have been significantly improved when the higher load of 50 N was applied as against 20 N for ABMC. The COF was greatly reduced at 50 N with 0.1168 for ABMC as against 20 N applied load with 0.4209. The wear volume (volume loss) was found to be 0.032578 mm^3 at 20 N for the fabricated AA7075-T651/17-4PH ABMC and 0.011374 mm^3 at 50 N which implies that less volume loss was achieved at higher load. The wear rate for the fabricated ABMC at 20 N was 10.859 mm^3/m and was recorded to be 2.275 mm^3/m while the wear resistance for the fabricated ABMC at 20 N applied load was 92086.66 m/mm^3 and was found to be 439599.09 m/mm^3 at 50 N force applied. From all indications, there exists tremendous improvement in the tribological properties of the fabricated ABMC. This scenario was also manifested at higher load than lower load for the parent material – AA7075-T651 as well as processed parent material (PPM) – FSPed AA7075-T651. The structural analysis also established that fabricated AA7075-T651/17-4PH has the lowest crystallite size of 37.4 nm followed by FSPed AA7075-T651 with 41.2 nm and lastly 48.7 nm for the parent material AA7075-T651, this shows that micro-particles of stainless steel has greatly influenced the grain refinement of the material and that ABMC has better structural integrity when compared to the control experiments. Many crystal phases were noticed on the peaks of AA7075-T651/17-4PH than what was noticed on the parent material peaks and that of the processed parent material. The Mechanical property was also noticed to be significantly improved with 613.58 MPa tensile strength and 622.22 MPa (ultimate tensile strength , UTS) for the fabricated AA7075-T651/17-4PH as against 559.07 MPa (tensile strength) and 603.83 MPa (UTS) for the processed FSPed AA7075-T651 while the parent material has 570.73 MPa tensile strength and 620.90 (UTS) which is higher than FSPed AA7075-T651. The fracture mechanism for AA7075-T651/17-4PH indicated that the fabricated ABMC was ductile having large volume of dimples-induced grain, exhibiting equiaxed dimples with prominent cup and cone features while there was brittle-ductile transition in the processed parent material – AA7075-T651/17-4PH with low ductility and Rock Candy fracture-like was noticed on the fracture surface and the parent material show elongated and large dimples with fibrous features, indicating ductility at low impact loading.

References

Akbari, M., Aliha, M. R. M., Keshavarz, S. M. E., & Bonyadi, A. (2019). Effect of tool parameters on mechanical properties, temperature, and force generation during FSW. *Proceedings of the Institution of Mechanical Engineers, Part L: Journal of Materials: Design and Applications*, *233*(6), 1033-1043.

Akbari, M., Shojaeefard, M. H., Asadi, P., & Khalkhali, A. (2017). Hybrid multi-objective optimization of microstructural and mechanical properties of B4C/A356 composites fabricated by FSP using TOPSIS and modified NSGA-II. *Transactions of Nonferrous Metals Society of China*, *27*(11), 2317-2333.

Aliha, M. R. M., Shahheidari, M., Bisadi, M., Akbari, M., & Hossain, S. (2016). Mechanical and metallurgical properties of dissimilar AA6061-T6 and AA7277-T6 joint made by FSW technique. *The International Journal of Advanced Manufacturing Technology*, *86*(9-12), 2551-2565.

Asadi, P., Givi, M. B., Rastgoo, A., Akbari, M., Zakeri, V., & Rasouli, S. (2012). Predicting the grain size and hardness of AZ91/SiC nanocomposite by artificial neural networks. *The International Journal of Advanced Manufacturing Technology*, *63*(9-12), 1095-1107.

Asuke, F., Abdulwahab, M., Aigbodion, V. S., Fayomi, O. S. I., & Aponbiede, O. (2014). Effect of load on the wear behaviour of polypropylene/carbonized bone ash particulate composite. *Egyptian Journal of Basic and Applied Sciences*, *1*(1), 67–70.

Baruwa, A. D., Oladijo, O. P., Maledi, N., & Akinlabi, E. T. (2018). Influence of surface treatment on dry sliding wear behavior of hydrophobic silane coating on AISI 304. *IOP Conference Series: Materials Science and Engineering*, *423*, 012158.

Behnagh, R. A., Besharati Givi, M. K., & Akbari, M. (2012). Mechanical properties, corrosion resistance, and microstructural changes during friction stir processing of 5083 aluminum rolled plates. *Materials and manufacturing processes*, *27*(6), 636-640.

Bhaskar, K. V., Sundarrajan, S., Rao, B. S., & Ravindra, K. (2018). Effect of reinforcement and wear parameters on dry sliding wear of Aluminum composites-A review. *Materials Today: Proceedings*,

5(2), 5891–5900.

Boromei, I., Ceschini, L., Morri, A., & Garagnani, G. L. (2006). Friction stir weldiong of Aluminium based composites reinforced with Al2O3 particles: Effects on microstructure. *Metallurgical Science and Technology*, *24*(1), 12–21.

Das, H., Mondal, M., Hong, S.-T., Chun, D.-M., & Han, H. N. (2018). Joining and fabrication of metal matrix composites by friction stir welding/processing. *International Journal of Precision Engineering and Manufacturing-Green Technology*, *5*(1), 151–172.

Deuis, R. L., Subramanian, C., & Yellup, J. M. (1997). Sliding wear of aluminum composites-A review. *Composites Science and Technology*, *3538*(96), 415–435.

Dinaharan, I, Kalaiselvan, K., Akinlabi, E. T., & Davim, J. P. (2017a). Microstructure and wear characterization of rice husk ash reinforced copper matrix composites prepared using friction stir processing. *Journal of Alloys and Compounds*, *718*, 150–160.

Dinaharan, I., Kalaiselvan, K., & Murugan, N. (2017b). Influence of rice husk ash particles on microstructure and tensile behavior of AA6061 aluminum matrix composites produced using friction stir processing. *Composites Communications*, *3*, 42-46.

Erinosho, M. F., Akinlabi, E. T., Pityana, S., Owolabi, G., Park, A., Campus, K., … Africa, S. (2017). Laser surface modification of Ti6Al4V-Cu for improved microhardness and wear resistance properties. *Materials Research.*, *20*(4), 1143–1152.

Fatchurrohman, N., Farhana, N., & Marini, C. D. (2018). Investigation on the effect of Friction Stir Processing Parameters on Micro-structure and Micro-hardness of Rice Husk Ash reinforced Al6061 Metal Matrix Composites. *IOP Conference Series: Materials Science and Engineering*, *319*(1), 0–6.

Feng, A. H., Chen, D. L., & Ma, Z. Y. (2010). Microstructure and cyclic deformation behavior of a friction-stir-welded 7075 al alloy. *Metallurgical and Materials Transactions A: Physical Metallurgy and Materials Science*, *41*(4), 957–971.

Garcia, C., Azpilgain, Z., Aginagalde, A., Esnaola, J. A., Galdos, L., & Torca, I. (2009). Tensile behaviour of 6082 Aluminium alloy sheet under different conditions of heat treatment, temperature and strain rate. *Key Engineering Materials*, *423*(February), 105–112.

Gerlich, A. P. (2017). Critical Assessment 25 : Friction stir processing , potential and problems Critical Assessment. *Materials Science and Technology*, *33*(10), 1139–1144.

Hao, Z., Fu, X., Men, X., & Zhou, B. (2019). Study on tensile and fracture properties of 7050-T7451 aluminum alloy based on material forming texture characteristics. *Materials Research Express*, *6*(3).

Huang, G., Hou, W., & Shen, Y. (2018). Evaluation of the microstructure and mechanical properties of WC particle reinforced aluminum matrix composites fabricated by friction stir processing. *Materials Characterization*, *138*(November 2017), 26–37.

Ikumapayi, O M, Ojolo, S. J., & Afolalu, S. A. (2015). Experimental and theoretical investigation of tensile stress distribution during Aluminium wire drawing. *European Scientific Journal*, *11*(18), 1857–7881. h

Ikumapayi, O. M., Okokpujie, I. P., Afolalu, S. A., Ajayi, O. O., Akilabi, E. T., & Bodunde, O. P. (2018). Effects of quenchants on impact strength of single-vee butt welded joint of mild steel. *IOP Conference Series: Materials Science and Engineering*, *391*, 1–10.

Ikumapayi, OM, Akinlabi, Esther T and Majumdar, J. D. (2019a). Influence of carbonaceous agrowastes nanoparticles on physical and mechanical properties of friction stir processed AA7075-T651 metal matrix composites. *Surface Topography: Metrology and Properties*, *7*(3), 1–17.

Ikumapayi, OM; Akinlabi, ET; Majumdar, JD; Akinlabi, S. (2019b). Characterization of high strength Aluminium – based surface matrix composite reinforced with low-cost PKSA fabricated by friction stir processing. *Materials Research Express*, *6*, 1–27.

Ikumapayi, Omolayo M, & Akinlabi, E. T. (2019). Experimental Data on Surface Roughness and Force Feedback Analysis in Friction Stir Processed AA7075 – T651 Aluminium Metal Composites. *Data in Brief*, https://doi.org/10.1016/j.dib.2019.103710.

Ikumapayi, Omolayo M, Akinlabi, E. T., & Majumdar, J. D. (2018a). Review on thermal, thermo-mechanical and thermal stress distribution during friction stir welding. *International Journal of Mechanical Engineering and Technology*, *9*(8), 534–548.

Ikumapayi, Omolayo M, Akinlabi, E. T., Pal, S. K., & Majumdar, J. D. (2019c). A survey on reinforcements used during friction stir processing of Aluminium metal matrix hybrid composites. *Procedia Manufacturing*, *35*, 935–940.

Ikumapayi, Omolayo M., & Akinlabi, E. T. (2019). Efficacy of α-β Grade titanium alloy powder (Ti-6Al-2Sn-2Zr-2Mo-2Cr-0.25Si) in surface modification and corrosion mitigation in 3.5% NaCl on friction stir processed armour grade 7075-T651 aluminum alloys - Insight in defence applications. *Materials Research Express*, *6*(7), 3–8.

Ikumapayi, Omolayo M., Oyinbo, S. T., Bodunde, O. P., Afolalu, S. A., Okokpujie, I. P., & Akinlabi, E. T. (2018b). The effects of lubricants on temperaturedistribution of 6063 aluminium alloy duringbackward cup extrusion process. *Journal of Materials Research and Technology*, *8*(1), 1175–1187.

Jain, S., Sharma, N., & Gupta, R. (2018). Dissimilar alloys (AA6082/AA5083) joining by FSW and parametric optimization using Taguchi, grey relational and weight method. *Engineering Solid Mechanics*, *6*(1), 51-66.

Jain, V. K. S., Muhammed, P. M., Muthukumaran, S., & Babu, S. P. K. (2018). Microstructure, mechanical and sliding wear behavior of AA5083–B4C/SiC/TiC surface composites fabricated using friction stir processing. *Transactions of the Indian Institute of Metals*, *71*(6), 1519–1529.

Jeyaprakash, N., Yang, C., Duraiselvam, M., & Prabu, G. (2019). Microstructure and tribological evolution during laser alloying WC-12 % Co and Cr 3 C 2 − 25 % NiCr powders on nodular iron surface. *Results in Physics*, *12*(December 2018), 1610–1620.

Johannes, L. B., & Mishra, R. S. (2007). Multiple passes of friction stir processing for the creation of superplastic 7075 aluminum. *Materials Science and Engineering A*, *464*(1–2), 255–260.

Kishan, V., Devaraju, A., & Prasanna Lakshmi, K. (2018). Tribological properties of nano TiB2particle reinforced 6061-T6 Aluminum alloy surface composites via friction stir processing. *Materials Today: Proceedings*, *5*(1), 1615–1619.

Koli, D. K., Agnihotri, G., & Purohit, R. (2014). A Review on Properties, Behaviour and Processing Methods for Al- Nano Al2O3 Composites. *Procedia Materials Science*, *6*(Icmpc), 567–589.

Kubit, A., Kluz, R., Trzepieciński, T., Wydrzyński, D., & Bochnowski, W. (2018). Analysis of the mechanical properties and of micrographs of refill friction stir spot welded 7075-T6 aluminium sheets. *Archives of Civil and Mechanical Engineering*, *18*(1), 235–244.

Kumar, K., Gulati, P., Gupta, A., & Shukla, D. K. (2017). A review of friction stir processing of aluminium alloys using different types of reinforcements. *Int. J. Mech. Eng. Technol*, *8*(7), 1638-1651.

Kumar, P., & Wani, M. F. (2017). Friction and wear behaviour of hypereutectic Al-Si alloy / steel tribopair under dry and lubricated conditions, *15*(June), 21–49.

Kundu, J., & Singh, H. (2017). Friction stir welding process: An investigation of microstructure and mechanical properties of Al Alloy AlMg4. 5Mn joint. *Engineering Solid Mechanics*, *5*(2), 145-154.

Kurgan, N. (2014). Investigation of the effect of diffusion bonding parameters on microstructure and mechanical properties of 7075 aluminium alloy. *The International Journal of Advanced Manufacturing Technology*, *71*(9–12), 2115–2124.

Mishra, R. S., & Ma, Z. Y. (2005). Friction stir welding and processing. *Materials Science and Engineering R: Reports*, *50*(1–2), 1–78.

Mishra, Rajiv Sharan, De, P. S., & Kumar, N. (2014). *Friction Stir Welding and Processing*. https://doi.org/10.1007/978-3-319-07043-8

Mistry, J. M., & Gohil, P. P. (2017). An overview of diversified reinforcement on aluminum metal matrix composites: Tribological aspects. *Proceedings of the Institution of Mechanical Engineers, Part J: Journal of Engineering Tribology*, *231*(3), 399–421.

Narasimharaju, S., & Sankunny, S. (2019). Microstructure and fracture behavior of friction stir lap welding of dissimilar AA 6060-T5/Pure copper. *Engineering Solid Mechanics*, *7*(3), 217-228.

Navaneethakrishnan, T., & Ganesh, P. (2015). Effect of welding parameters on friction stir welded dissimilar aluminum alloys 7075 and 6082 with various tool pin profiles. *Journal of Chemical and Pharmaceutical Sciences*, *2015-April*(9), 463–468.

Offor, P. O., Okorie, B. A., Ezema, F. I., Aigbodion, V. S., & Daniel-mkpume, C. C. (2015). Synthesis and characterization of nanocrystalline zinc sulphide thin fi lms by chemical spray pyrolysis. *Journal of Alloys and Compounds*, *650*, 381–385.

Padhy, G. K., Wu, C. S., & Gao, S. (2017). Friction stir based welding and processing technologies - processes, parameters, microstructures and applications: A review. *Journal of Materials Science and Technology*, *34*, 1–38.

Pandey, V., Singh, J. K., Chattopadhyay, K., Srinivas, N. C. S., & Singh, V. (2017). Influence of ultrasonic shot peening on corrosion behavior of 7075 aluminum alloy. *Journal of Alloys and Compounds*, *723*, 826–840.

Patel, V. V., Badheka, V., & Kumar, A. (2017). Effect of polygonal pin profiles on friction stir processed superplasticity of AA7075 alloy. *Journal of Materials Processing Technology*, *240*, 68–76.

Rambabu, P., Prasad, N. E., & Kutumbarao, V. V. (2017). Aerospace materials and material technologies. https://doi.org/10.1007/978-981-10-2143-5

Rana, H. G., Badheka, V. J., & Kumar, A. (2016). Fabrication of Al7075 / B4C Surface Composite by Novel Friction Stir Processing (FSP) and Investigation on Wear Properties. *Procedia Technology*, *23*, 519–528.

Sanusi, K. O., & Akinlabi, E. T. (2017). Friction-stir processing of a composite aluminium alloy (AA 1050) reinforced with titanium carbide powder. *Materiali in Tehnologije*, *51*(3), 427–435.

Selvakumar, S., Dinaharan, I., Palanivel, R., & Babu, B. G. (2017). Development of stainless steel particulate reinforced AA6082 aluminum matrix composites with enhanced ductility using friction stir processing. *Materials Science and Engineering A*, *685*(January), 317–326.

Sert, A., & Celik, O. N. (2014). Wear behavior of SiC-reinforced surface composite Al7075-T651 aluminum alloy produced using friction stir processing. *Indian Journal of Engineering & Materials Sciences*, *21*(February), 35–43.

Shahraki, S., Khorasani, S., Behnagh, R. A., Fotouhi, Y., & Bisadi, H. (2013). Producing of AA5083/ZrO 2 nanocomposite by friction stir processing (FSP). *Metallurgical and Materials Transactions B*, *44*(6), 1546-1553.

Sharma, A., Sharma, V. M., Sahoo, B., Joseph, J., & Paul, J. (2018). Study of nano-mechanical, electrochemical and raman spectroscopic behavior of Al6061-SiC-Graphite hybrid surface composite fabricated through friction stir processing. *Journal of Composites Science*, *2*(32), 1–17.

Sharma, V., Prakash, U., & Kumar, B. V. M. (2015). Surface composites by friction stir processing: A review. *Journal of Materials Processing Technology*, *224*, 117–134.

Shojaeefard, M. H., Akbari, M., Asadi, P., & Khalkhali, A. (2017). The effect of reinforcement type on the microstructure, mechanical properties, and wear resistance of A356 matrix composites produced by FSP. *The International Journal of Advanced Manufacturing Technology*, *91*(1-4), 1391-1407.

Sudhakar, D., Jeyasimman, D., & Duraiselvam, M. (2015). Dry sliding wear behavior of Cr 3 C 2 -NiCr coating on austenitic stainless steel. *International Journal Of Core Engineering & Management*, *1*(12), 215–225.

Sudhakar, I., Madhu, V., Madhusudhan Reddy, G., & Srinivasa Rao, K. (2015). Enhancement of wear and ballistic resistance of armour grade AA7075 aluminium alloy using friction stir processing. *Defence Technology*, *11*(1), 10–17.

Sudhakar, I., Madhusudhan Reddy, G., & Srinivasa Rao, K. (2016). Ballistic behavior of boron carbide reinforced AA7075 aluminium alloy using friction stir processing – An experimental study and analytical approach. *Defence Technology*, *12*(1), 25–31.

Taheri-Behrooz, F., Aliha, M. R., Maroofi, M., & Hadizadeh, V. (2018). Residual stresses measurement in the butt joint welded metals using FSW and TIG methods. *Steel and Composite Structures*, *28*(6), 759-766.

Torabi, A. R., Kalantari, M. H., & Aliha, M. R. M. (2018). Fracture analysis of dissimilar Al-Al friction stir welded joints under tensile/shear loading. *Fatigue & Fracture of Engineering Materials & Structures*, *41*(9), 2040-2053.

Torabi, A. R., Kalantari, M. H., Aliha, M. R. M., & Ghoreishi, S. M. N. (2019). Pure mode II fracture analysis of dissimilar Al-Al and Al-Cu friction stir welded joints using the generalized MTS criterion. *Theoretical and Applied Fracture Mechanics*, *104*, 102369.

Vasco, M., Tserpes, K., & Pantelakis, S. (2018). Numerical simulation of tensile behavior of corroded Aluminum alloy 2024 T3 considering the hydrogen embrittlement. *Metals*, *8*(1), 56.

Vijaya Kumar, P., Madhusudhan Reddy, G., & Srinivasa Rao, K. (2015). Microstructure and pitting corrosion of armor grade AA7075 aluminum alloy friction stir weld nugget zone – Effect of post weld heat treatment and addition of boron carbide. *Defence Technology*, *11*(2), 166–173.